

# Assembly of *Acanthamoeba* Myosin-II Minifilaments. Model of Anti-parallel Dimers Based on EM and X-ray Diffraction of 2D and 3D Crystals

Kirsi Turbedsky<sup>1</sup>, Thomas D. Pollard<sup>1</sup> and Mark Yeager<sup>2,3\*</sup>

<sup>1</sup>Structural Biology Laboratory  
Salk Institute for Biological  
Studies, 10010 North Torrey  
Pines Road, La Jolla, CA 92037  
USA

<sup>2</sup>Department of Cell Biology  
Scripps Research Institute  
10550 North Torrey Pines Road  
La Jolla, CA 92037, USA

<sup>3</sup>Division of Cardiovascular  
Diseases, Scripps Clinic, 10666  
North Torrey Pines Road  
La Jolla, CA 92037, USA

Current models suggest that the first step in the assembly of *Acanthamoeba* myosin-II is anti-parallel dimerization of the coiled-coil tails with an overlap of 15 nm. Sedimentation equilibrium experiments showed that a construct containing the last 15 heptads and the non-helical tailpiece of the myosin-II tail (15T) forms dimers. To examine the structure of the 15T dimer, we grew 3D and 2D crystals suitable for X-ray diffraction and electron image analysis, respectively. For both conditions, crystals formed in related space and plane groups with similar unit cells ( $a = 87.7 \text{ \AA}$ ,  $b = 64.8 \text{ \AA}$ ,  $c = 114.9 \text{ \AA}$ ,  $\beta = 108.0^\circ$ ). Inspection of the X-ray diffraction pattern and molecular replacement analysis revealed the orientation of the coiled-coils in the unit cell. A 3D density map at 15 Å in-plane resolution derived from a tilt series of electron micrographs established the solvent content of the 3D crystals (75%, v/v), placed the coiled-coil molecules at the approximate translation in the unit cell, and revealed the symmetry relationships between molecules. On the basis of the low-resolution 3D structure, biochemical constraints, and X-ray diffraction data, we propose a model for myosin interactions in the anti-parallel dimer of coiled-coils that guide the first step of myosin-II assembly.

© 2004 Elsevier Ltd. All rights reserved.

**Keywords:** myosin; coiled-coil; assembly; X-ray crystallography; electron microscopy

\*Corresponding author

## Introduction

Non-muscle motile cells contain myosin-II in small minifilaments generally concentrated at the rear of locomoting cells or in the cleavage furrow during cytokinesis. In *Acanthamoeba*, these minifilaments have been identified as bipolar octamers that are 230 nm long with a 117 nm bare zone and 15.5 nm stagger between myosin heads.<sup>1</sup> The simple structure of the minifilaments made it possible to characterize the assembly steps in greater detail than possible with large muscle thick filaments. Sinard *et al.*<sup>1,2</sup> used electron microscopy to visualize assembly intermediates and mapped important interaction sites using

recombinant protein expression and monoclonal antibody binding.<sup>3</sup> In the accompanying paper, we show that the last 32 of 90 heptads suffice for octamer formation while constructs with the last 14 heptads form anti-parallel dimers.<sup>4</sup> Therefore, the distal part of the amoeba myosin-II tail contains all of the information required for assembly.

The *Acanthamoeba* myosin-II coiled-coil tail contains 90 heptads and forms an 87 nm rod. Although there is no unique way to align the *Acanthamoeba* sequence with other myosin sequences, there is conservation in the heptad repeat, as well as the 28 residue zones containing alternating regions of positive and negative charges.<sup>5</sup> These charged residues on the surface of the coiled-coil tail are thought to determine the stagger between myosins within a filament.<sup>6–8</sup>

The assembly process of *Acanthamoeba* myosin-II is relevant to non-muscle systems and has similarities to skeletal and smooth muscle myosin. Skeletal muscle assembly appears to involve a nucleating structure similar to *Acanthamoeba* octameric minifilaments.<sup>9,10</sup> In addition, most myosins have an assembly-competent domain

Present address: Thomas D. Pollard, Department of Molecular, Cellular and Developmental Biology, Yale University, New Haven, CT 06520, USA.

Abbreviations used: MIR, multiple isomorphous replacement; MAD, multiple anomalous dispersion; EM, electron microscopy.

E-mail address of the corresponding author: yeager@scripps.edu

consisting of 29 residues of the coiled-coil rod near the C terminus.<sup>11–14</sup> In the case of *Acanthamoeba* myosin-II, the non-helical tailpiece fulfils a similar role, since assembly does not occur in the absence of the tailpiece.<sup>2,3,15</sup>

Although the structure of skeletal muscle myosin thick filaments has been studied extensively using electron microscopy and low-angle fiber diffraction,<sup>16–19</sup> the 3D packing and specific interactions that direct the formation of myosin filaments are unknown. To explore the assembly mechanism of myosin filaments, we examined 2D and 3D crystals derived from a construct designated 15T that consists of the last 137 residues of *Acanthamoeba* myosin-II. The accompanying paper demonstrates that 15T forms high-affinity dimers in solution.<sup>4</sup> Here, we show that construct 15T forms diffraction-quality 2D and 3D crystals. On the basis of a low-resolution 3D structure derived by electron crystallography, as well as biochemical constraints and X-ray diffraction data, we propose a model for myosin interactions in the anti-parallel dimer of coiled-coils that guide the first step of myosin-II assembly.

## Results

To examine the assembly mechanism of myosin-II, we generated a series of ten different N-terminal truncation constructs of *Acanthamoeba* myosin-II, which are named according to the number of heptad repeats prior to the C terminus. Construct 32T forms octamers, while constructs 14T through 22T form dimers in solution. Constructs smaller than 12T did not assemble into coiled-coils.<sup>4</sup>

### The 3D crystallization trials

Most constructs did not yield crystals that diffracted to high resolution. For instance, constructs 32T and 22T formed long and thin, rubbery crystals that diffracted weakly. Construct 20T formed fine strands of crystalline material that were too small to test for diffraction. Constructs 12T and 14T crystallized into small rectangular cubes but diffracted poorly. Constructs 6T and 8T did not

crystallize under any conditions tried, in spite of extensive screening.

Construct 15R (lacking the tailpiece) formed very large diamond-shaped crystals ( $300\ \mu\text{m} \times 300\ \mu\text{m} \times 300\ \mu\text{m}$ ) at  $15\ ^\circ\text{C}$  in 15% (w/v) PEG 400, 0.1 M Tris (pH 8.5) or in 7% (w/v) PEG 8000, 0.1 M imidazole (pH 6.5). In spite of the large well-formed crystals, diffraction did not extend beyond  $4\ \text{\AA}$  under any conditions studied. Construct 15R crystallized in space group *I4* with a unit cell of  $a=109.2\ \text{\AA}$ ,  $b=109.2\ \text{\AA}$ ,  $c=295.0\ \text{\AA}$  (Table 1). On the basis of the unit cell volume and size of 15R, the asymmetric unit may contain anywhere between four and eight monomers corresponding to a solvent content of 40–70% (v/v).

Similar to 15R, construct 15T crystallized overnight in 10% PEG 400, 0.1 M Tris (pH 8.5) at  $15\ ^\circ\text{C}$ . However, the morphology was quite different. The initial thin, plate-like crystals did not diffract, but addition of formic acid to the protein drop allowed slow pH equilibration with the reservoir and enabled slower growth of the crystals. These crystals were much thicker and produced the most promising diffraction patterns. Construct 15TC (lacking the last seven residues) formed identical crystals under these conditions.

### X-ray data collection

Construct 15T crystallized in space group *C2* with unit cell dimensions of  $a=87.7\ \text{\AA}$ ,  $b=64.8\ \text{\AA}$ ,  $c=114.9\ \text{\AA}$ ,  $\beta=108.0^\circ$  (Table 1). Construct 15TC crystallized with the same space group and unit cell parameters. Based on the unit cell size, the asymmetric unit was sufficient to contain two molecules of 15T with a solvent content of 50% (v/v), or one molecule with a solvent content of 75% (v/v). Sufficiently large 3D crystals of 15T ( $200\ \mu\text{m} \times 200\ \mu\text{m} \times 50\ \mu\text{m}$ ) diffracted X-rays anisotropically, with an intensity distribution typical of oriented coiled-coils like tropomyosin.<sup>20</sup> Diffraction patterns obtained from the face of the crystals showed spots at  $10\ \text{\AA}$  and at  $5\ \text{\AA}$  resolution with very weak diffraction in between, while a more uniform pattern was obtained along the thickness of the crystal (Figure 1(a)). A strong meridional reflection at  $5.1\ \text{\AA}$  corresponded to the  $\alpha$ -helical pitch shortened from

**Table 1.** Native X-ray diffraction data collection statistics

	15T	15TC	15R	15R
Source	SSRL	SSRL	Salk	SSRL
Wavelength ( $\text{\AA}$ )	1.08	1.08	1.542	1.08
Space group	C2	C2	I4	I4
Unit cell dimensions				
$a$ ( $\text{\AA}$ )	87.69	87.98	108.5	109.2
$b$ ( $\text{\AA}$ )	64.80	64.21	108.5	109.2
$c$ ( $\text{\AA}$ )	114.88	114.41	295.2	295.0
$\beta$ (deg.)	108.04	108.30	90.0	90.0
Resolution ( $\text{\AA}$ )	3.5	3.4	4.0	50–4.0
$R_{\text{merge}}$				
Overall	5.6	8.3	13.2	10.7
Last bin	20.5	18.8	17.8	16.5
Completeness (%)	94.0	93.1	99.3	97.5

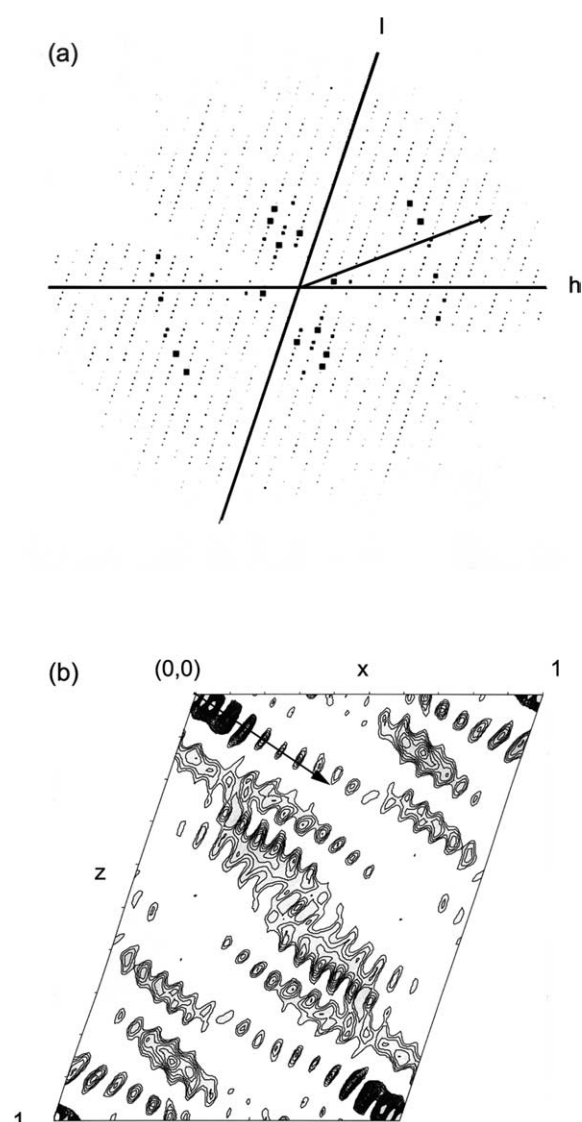


**Figure 1.** (a) Pseudo-precession plot of the measured X-ray diffraction intensities from native 3D 15T crystals collected at SSRL and calculated using the CCP4 program HKLVIEW. Strong reflections in the  $(h,0,l)$  plane suggest that the coiled-coils lie in the  $k=0$  plane. The helices are oriented  $\sim 20^\circ$  from the  $h$  axis in reciprocal space (marked by an arrow) with characteristic meridional reflections at 5.1 Å and near-equatorial reflections at 10 Å. The limit of diffraction is 2.8 Å. (b) Native Patterson map of construct 15T calculated and displayed using the xfft and xcontur modules of XTALVIEW. Strong repeating peaks in the  $y=0$  plane occur along an angle of  $74^\circ$  from the  $z$ -axis ( $-34^\circ$  from the  $x$ -axis) (marked by the arrow) and correspond to the vectors between residues along the  $\alpha$ -helical coiled-coil.

its normal length of 5.4 Å due to the left-handed supercoiling of the coiled-coil.<sup>21,22</sup>

Native X-ray data provided information on the packing of the myosin molecules in the 3D crystals. Normally, native Patterson maps lack distinguishable features because most of the interatomic self-vectors cancel to produce characteristic weak

signals suitable only for computational searches. However, the native Patterson map of the 15T data had very strong repeating features (Figure 1(b)), particularly in the  $y=0$  plane. We attributed this to parallel packing of coiled-coils along an angle of  $72^\circ$  from the  $z$ -axis in which the self vectors are additive. The series of peaks occurred at 5.1 Å increments, which corresponded to the pitch of an  $\alpha$ -helix in a coiled-coil. In addition, a strong peak was present along this series of peaks at 75 Å, presumably due to the interatomic vectors that are one half pitch long.<sup>20,23,24</sup> Self-rotation analysis also identified a 2-fold axis along this direction. The 3D Patterson map suggested that the molecules lie almost flat in the  $(x,z)$  plane. In summary, the diffraction pattern, the self-rotation function, and the native Patterson map suggested that: (1) the coiled-coils lie flat in the  $(x,z)$  plane; (2) they are oriented at an angle of  $72^\circ$  from the  $z$ -axis; (3) the molecules pack parallel in the crystal (not crossing at an angle); and (4) the pitch of the coiled-coil is  $\sim 150$  Å.

Since we were unable to obtain experimental phases from standard multiple isomorphous replacement (MIR) and multiple anomalous dispersion (MAD) phasing techniques (see Materials and Methods), we attempted to solve the structure of 15T by molecular replacement with a search model based on the high-resolution crystal structures of the GCN4<sup>25</sup> and cortexillin coiled-coils.<sup>26</sup> Calculation of the electrostatic potential of construct 15T revealed patches of positive and negative charge (Figure 5), as expected from the known 29 residue repeat.<sup>5</sup> The positive patch was located in the region of the skip residue at position 1418 and included several positively charged residues in the  $a$  and  $d$  positions of the coiled-coil heptad repeat. This encompassed two positive regions as designated by the 28 residue repeat. The negative patch surrounded a glycine residue at position 1459 and did not include any positively charged residues.

Automated molecular replacement programs produced solutions with high correlation coefficients ( $\sim 0.3$ ) but also very high  $R$ -factors ( $\sim 0.55$ ). Although the solutions had similar scores and the same longitudinal rotation of the rod, there was no unique transverse rotation or translation solution. Using AMoRe,<sup>5</sup> all of the highest ranked solutions positioned the coiled-coils in the  $(x,z)$  plane at the same angle as observed in native Patterson maps, but there were differences in the azimuthal rotation, the translation sliding along the coiled-coil length, and/or the translation in the  $(x,z)$  plane. Programs CNS and EPMR (see Materials and Methods) also yielded a similar family of solutions. In conjunction with molecular replacement we employed multiple rounds of solvent flipping and flattening using CNS and a solvent content of 75% but were unable to identify a single best solution.

## The 2D crystallization trials

Since our phasing attempts were stymied and a

unique solution could not be derived by molecular replacement methods, we reasoned that direct visualization of the crystals might reveal packing information that would provide constraints for molecular replacement. Our 2D crystallization trials were focused on 15T, since this construct formed thin crystals rapidly. The strategy was to grow 2D crystals of 15T directly on electron microscopy (EM) grids using conditions similar to those used for 3D crystallization but excluding formic acid: 6% PEG 400 and 67 mM Tris (pH 8). Negatively stained samples showed clusters of thin, oval-shaped

patches of varying thickness and a diameter between 0.5  $\mu\text{m}$  and 2  $\mu\text{m}$  (Figure 2(a)). At a magnification of 52,000 $\times$ , a visible repeating lattice confirmed that the patches were indeed crystalline. Stairstepping at the edges suggested that the patches were comprised of multi-layered crystals, not suitable for electron crystallography. However, in the vicinity of the densely stained thick crystals were some crystals with lower optical density, suggesting that they were formed by just a few layers. Decreasing the incubation time for crystallization resulted in thin, single-layered crystals.

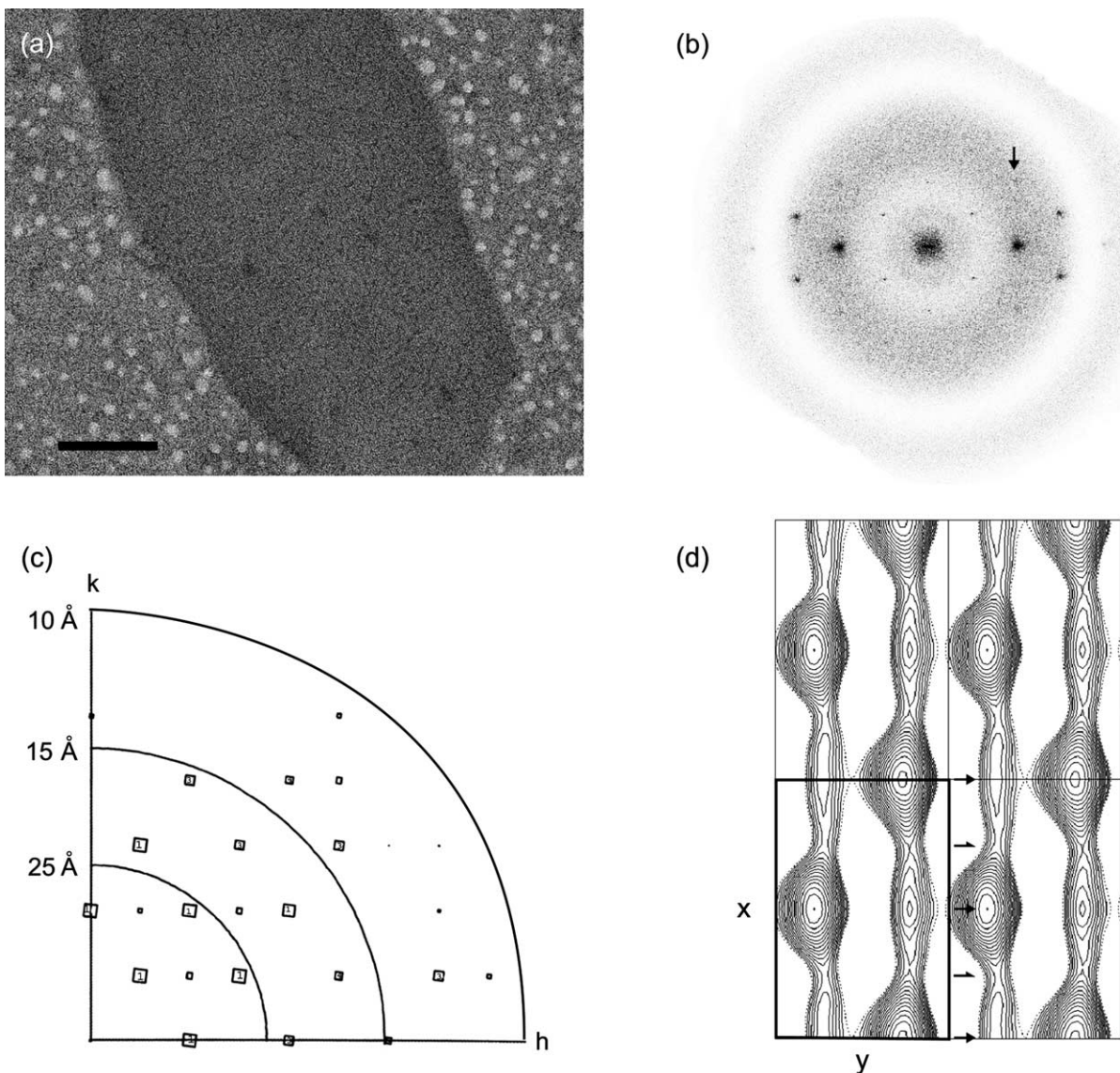


**Figure 2.** (a) A low-dose transmission electron micrograph recorded at a magnification of 30,000 $\times$  showing a representative myosin-II 15T 2D crystal negatively stained with uranyl acetate (the scale bar represents 1000 Å). (b) The computed diffraction pattern of the image shown in (a) displays diffuse (2,0) reflections and clearly visible (2,2) reflections (arrow). (c) Combined phase error for each unique reflection to 10 Å after vectorial averaging of the merged data from ten separate 15T 2D crystals. The size of the boxes reflects the accuracy of the error associated with each structure factor ( $1 < 8^\circ$ ,  $2 < 14^\circ$ ,  $3 < 20^\circ$ ,  $4 < 30^\circ$ ,  $5 < 40^\circ$ ,  $6 < 50^\circ$ ,  $7 < 70^\circ$ ). For clarity, only the boxes sized from 1 to 4 are numbered, and a decreasing box size is used for numbers 5–7. The reflections with a mean phase error larger than  $70^\circ$  have been excluded. For this calculation,  $90^\circ$  represents a random phase error. (d) The projection density map at 15 Å resolution of the myosin-II 15T construct in plane group  $c12$  with symmetry operators as shown. A single unit cell ( $a = 89.1$  Å,  $b = 65.5$  Å) is outlined in bold and contains two myosin-II dimers of coiled-coils.

## Electron microscopy

Only  $\sim 10\%$  of the thinnest patches displayed optical diffraction. The strong (2, 0) reflection was typically very diffuse (Figure 2(b)). We attributed this spot to the 65 Å packing between the molecules. The (1, 3) reflection was also quite strong but much less diffuse. While the (1, 1) and (2, 0) spots were often visible, only the best-ordered crystals displayed the (2, 2) reflection. Therefore, we considered only those crystals with (2, 2) reflections for image processing.

Computed diffraction patterns of large, single-layered 2D crystals (Figure 2(c)) showed that the unit cell and plane group were identical, within experimental error, with the ( $x, y$ ) plane of the 3D crystals. However, the X-ray data of the 3D crystals suggested that the coiled-coils were lying flat in the ( $x, z$ ) plane. Since the 2D crystals formed in the ( $x, y$ ) plane, the projection map (Figure 2(d)) did not clearly reveal the packing of the coiled-coils, as it may have if the 2D crystals had corresponded to the ( $x, z$ ) plane. In space group  $C2$ , the translation in the  $y$  direction is arbitrary, so the location of the coiled-coils in the ( $x, y$ ) plane observed in the projection map did not provide any new information.

To understand the packing of the coiled-coils, a 3D reconstruction was derived by merging diffraction data from images of the 2D crystals at tilt angles between  $0^\circ$  and  $55^\circ$  (Figure 3). The dominant feature was a corrugated rod of density  $\sim 130$  Å long

(Figure 4). A 2-fold symmetry axis through the center created identical halves of the molecule. The transverse cross-section of the density was elliptical and of sufficient size ( $20 \text{ Å} \times 43 \text{ Å}$ ) to accommodate two coiled-coils, side-by-side (Figure 4(c)). The rods of density were packed in a parallel fashion at an angle of  $70^\circ$  with respect to the surface of the EM grid. Since the other half of the dimer was created by symmetry, only one 15T molecule was present in the asymmetric unit. We note that a coiled-coil model would form a fairly smooth rod at low resolution, whereas the density map shows distinctive thick and thin features. Analysis of the point-spread function suggested that the resolution was 13.7 Å in the plane of the 2D crystals and 35 Å in  $z$ . In spite of the low resolution of the map, the beads of density are spaced too far apart to be due to Fourier series termination artifacts. Rather, we suspect that the beads of density arise from the distribution of negative stain on the surface of the coiled-coils. Negative stain has a tendency to accumulate in hydrophilic regions on the surface of proteins.<sup>27</sup> The 15T coiled-coil dimer has distinctive patches of acidic and basic residues (Figure 5), and the puddling of stain in these regions may give rise to the thin, scalloped zones in the EM map.

## Combining EM and X-ray data

The unit cell and space group suggested identical

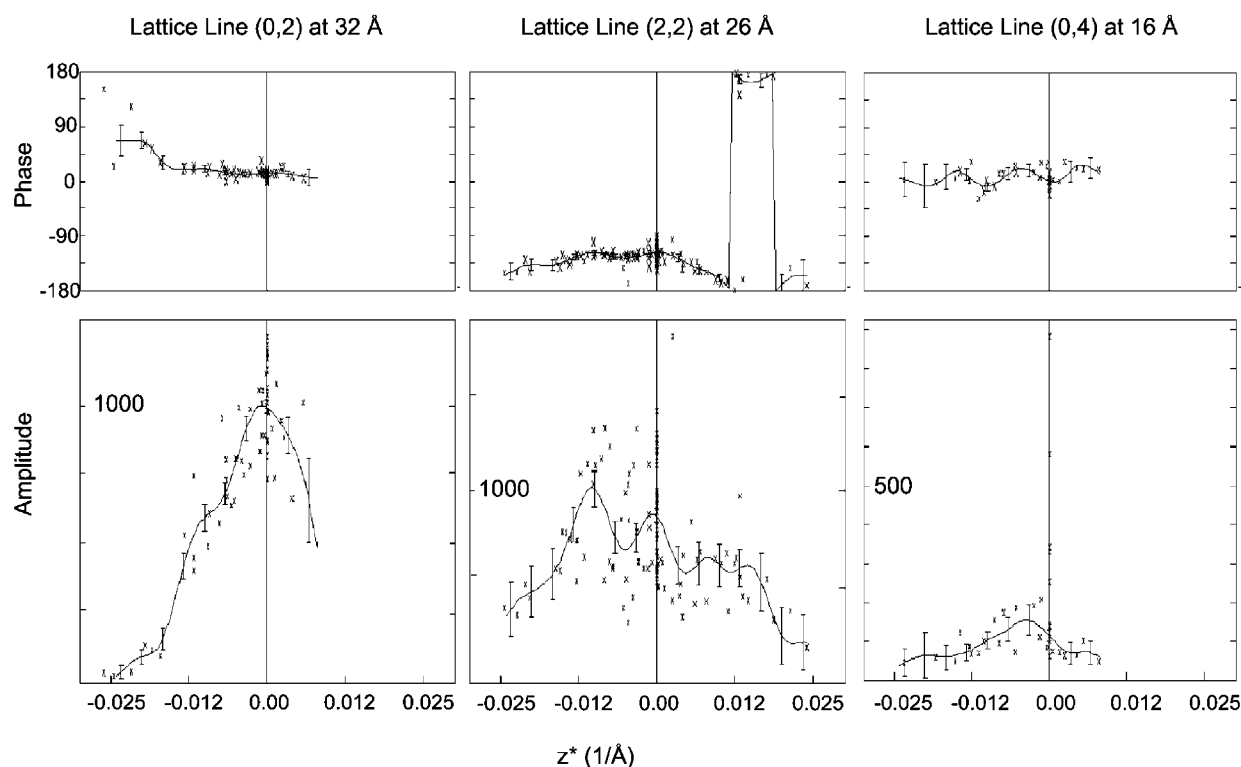


**Figure 3.** Amplitude and phase variations along selected lattice lines after merging data from tilted crystals in the two-sided plane group  $c12$ . The points include all data with a signal-to-noise ratio  $> 1$  (IQ 8 and better). The continuous curves were computed by the program LATLINE. The horizontal  $z^*$  axis is the distance from the origin of the lattice line. Error bars, SD of phases and amplitudes for the fitted structure factor.

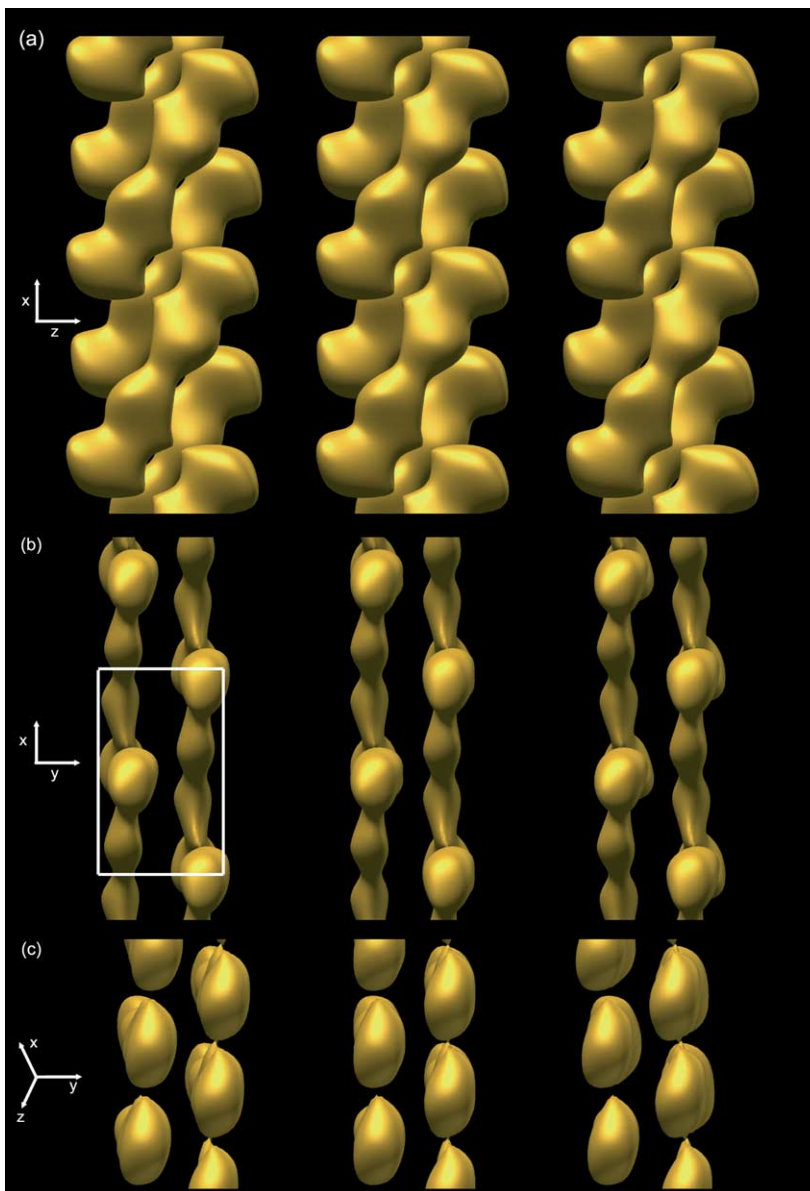


**Figure 4.** The 3D reconstruction of the myosin-II 15T construct. (a) The  $(x,z)$  plane shows the side-by-side packing of the molecules in the 2D crystals and corresponds to the  $y=0$  view of the native Patterson in Figure 1(b). (b) The  $(x,y)$  plane shows the overlapping stacking of the molecules and corresponds to the projection map in Figure 2(d). The boxed area corresponds to one unit cell. (c) A  $60^\circ$  rotation of (b) around  $y$  provides an end-on view of the molecules and shows the oval shape of the 3D reconstruction sufficient to accommodate two coiled-coils. The left-hand and right-hand pairs are wall-eyed and cross-eyed stereo views, respectively.

packing in the 2D and 3D crystals. In addition, the orientation of the molecule in the 2D unit cell observed in the EM reconstruction matched the angle observed in the 3D X-ray diffraction data, native Patterson maps and molecular replacement solutions. Based on the EM reconstruction, there is only one 15T coiled-coil present in the asymmetric unit of the 3D crystal. Therefore, the solvent content of the 3D crystal of 15T was 75%, similar to crystals of other long coiled-coil proteins such as tropomyosin<sup>20</sup> and cortexillin,<sup>28</sup> but higher than we estimated initially. The high solvent content may account for the difficulties in growing and manipulating the crystals, particularly in their sensitivity to changing solution conditions and temperatures. The EM reconstruction indicated that there was only one coiled-coil per asymmetric unit and that the anti-parallel dimer was formed by the crystallographic axis. Therefore, there were a limited number of possible positions for the coiled-

coil in the unit cell. These constraints were used for another attempt at molecular replacement. The coiled-coil was placed only where anti-parallel symmetry mates produced low-resolution density  $\sim 40$  Å wide. The EM density dictated that the two coiled-coils were oriented side-by-side within the  $(x,z)$  plane.

The best molecular replacement solution from CNS placed the coiled-coil model near the center of the EM density. The cross-validated  $\sigma$ -weighted  $2F_o - F_c$  map from the model in CNS displayed density where the model was placed. To identify additional protein density, we performed density modification using either the actual dimensions of the EM map or a longer mask containing the expected protein based on the GCN4 model. The resulting maps contained better-defined helical regions and additional side-chain density.

After testing all these possibilities, the model with the lowest  $R$ -factor was obtained by placing

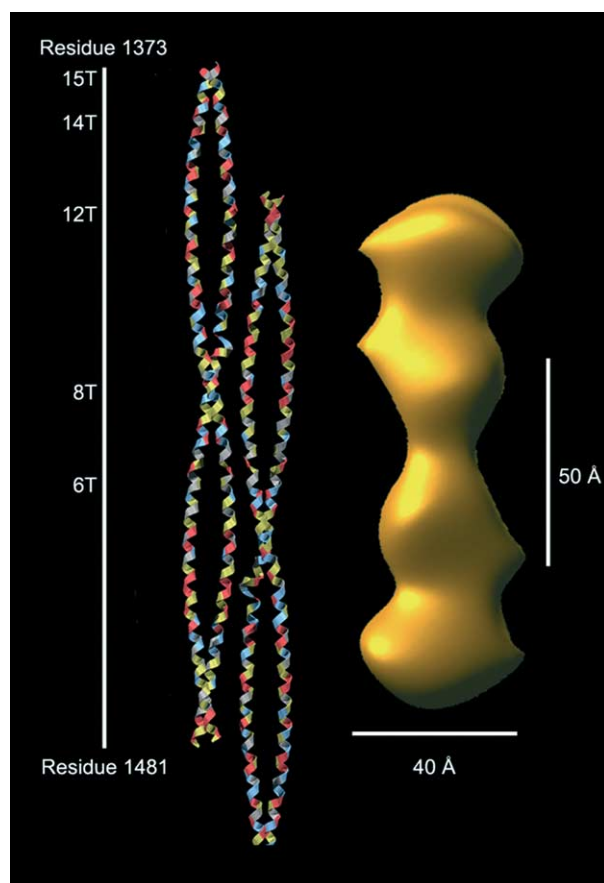


**Figure 5.** Comparison of the 3D reconstruction of the myosin-II coiled-coil dimer (right) to a hypothetical coiled-coil ribbon model of the anti-parallel 15T dimer created by a 2-fold symmetry axis that matches the regions of opposite charge (left). The scale at the left shows the relative lengths of constructs (6T–15T) tested for assembly in the accompanying paper.<sup>4</sup>

the coiled-coil model over the location of individual chains moved by simulated annealing. Even though we obtained models with lower *R*-factors than those obtained by simply placing a coiled-coil molecule by hand in the EM density, the final *R*-factor for the best, most sensible model was still 0.49 with a free *R*-factor of 0.55. Although the  $\alpha$ -helical packing arrangement of this model is likely to be correct, our analysis did not provide any information about the conformation of the 29 residue tailpiece.

## Discussion

### X-ray diffraction suggests parallel packing of coiled-coils in the myosin II construct 15T

X-ray diffraction of oriented  $\alpha$ -helical coiled-coils as found in the 3D crystals of construct 15T presents a case where much information can be gained directly from the native data itself. Interpretation of the diffraction pattern, self-rotation function, and

Patterson maps revealed strong constraints about the molecular packing in the absence of any phasing information. The native Patterson map was particularly informative. Due to the alignment of  $\alpha$ -helices in the coiled-coil, the interatomic vectors within the helix sum to form a significant peak in the native Patterson map. In the case of 15T, all coiled-coils lie parallel with each other and produce a single peak. The repeating series of peaks in the native Patterson maps, the fiber-like diffraction pattern in the  $h0l$  plane of the pseudo-precession plots, the non-crystallographic 2-fold signal in the self-rotation function, and the family of molecular replacement solutions suggested that the coiled-coils are parallel with each other and lie flat in the  $y=0$  plane at a  $70^\circ$  angle from  $z$ .

### Electron crystallography revealed anti-parallel coiled-coil association of 15T dimers

The low-resolution 3D map derived by electron crystallography provided direct visualization of this packing arrangement of the coiled-coils in the unit cell. The reconstruction is centered on the crystallographic 2-fold symmetry axis in the ( $x,z$ ) plane. This creates EM density with cross-sectional dimensions sufficient to include two coiled-coil molecules side-by-side. Placement of one coiled-coil model in half of the EM density establishes the position of another molecule aligned with the first but rotated  $180^\circ$  as dictated by 2-fold symmetry. This shows that construct 15T crystallizes as a dimer of coiled-coils, as expected from its assembly properties determined by sedimentation equilibrium.<sup>3</sup> Symmetry relationships in the EM structure require that the two coiled-coils are anti-parallel, as predicted by the first step in the established assembly pathway. The EM density is  $\sim 130$  Å long, somewhat shorter than the  $\sim 150$  Å observed in electron micrographs of metal-shadowed dimers of whole myosin.<sup>29</sup> This length suggests that the 15T coiled-coil is fully overlapped in the dimers.

The unit cell and orientation of the coiled-coil density in the EM map showed that the 2D crystal is simply a single layer of the 3D crystal. Consequently, direct structural comparisons can be made. The 3D EM map shows that the asymmetric unit contains a single coiled-coil and constrains the location of the coiled-coil dimer in the unit cell of the 3D crystals. This coiled-coil is located near the crystallographic symmetry axis, such that an anti-parallel dimer is formed by the C2 symmetry. Since the low-resolution density is  $\sim 40$  Å wide, the possible positions in which to place the coiled-coil in the unit cell are also limited. Therefore, the EM structure was very helpful in defining the position of the coiled-coils in the 3D crystals and interpreting the X-ray diffraction data. Nevertheless, we were unable to phase the X-ray diffraction data using this information with a coiled-coil model alone. Several factors contributed to this difficulty. First, the data were limited in both resolution and intensity.

Second, our coiled-coil model may not be sufficiently close to the actual structure to yield accurate phases. For example, the 29 residue non-helical tailpiece may distort the canonical coiled-coil structure of 15 heptads. Third, oriented coiled-coils can be very difficult to place unambiguously in the unit cell in the absence of independent phase information, as exemplified by Whitby's work on tropomyosin.<sup>30</sup>

### A model for the 15T coiled-coil dimer

Biophysical studies other than the structural work described here provide important clues for modeling the molecular interactions in myosin-II dimers. Electron microscopy of full-length myosin-II dimers showed that the two anti-parallel coiled-coils overlap  $\sim 150$  Å.<sup>29</sup> Assembly experiments showed that the last 14 or 15 heptads are required for dimerization of the myosin-II tail. The dramatic salt-dependence on oligomer formation suggested that ionic interactions play a major role in assembly. On the basis of these results and our crystallographic analysis, we propose a model for the anti-parallel dimer of 15T using the 2-fold symmetry observed in the 3D reconstruction, and assuming interaction of the cationic and anionic regions, as depicted in the ribbon rendering in Figure 5. A coiled-coil model of myosin-II was translated to a position along the best molecular replacement solution that produced the greatest overlap between the negatively charged patch at residues 1412–1427 and the positive patch at 1455–1463. The rotation of the rod was chosen such that the major negative patch faced the interior of the dimer interface. In addition, we chose the azimuthal orientation of the two coiled-coils to bury Phe1443, since the environment of a tryptophan substitution at this position changes upon dimerization.<sup>4</sup> This model takes into account the electrostatic nature of the interaction, the assembly properties of truncation mutants, and the low-resolution 3D map derived by electron crystallography. There is juxtaposition of the charged patches, and the transverse rotation can be adjusted so that the grooves and ridges of the coiled-coil fit into each other. Although the *R*-factor for this model remains similar to molecular replacement solutions (49%), the model agrees well with all other biochemical information.

This model has many encouraging features. First, the anti-parallel overlap of the coiled-coils is  $\sim 130$  Å, the total length of the EM density (Figure 5). The 130 Å overlap allows for  $\sim 20$  Å of overhang. This overhang presumably interacts with the 29 residue non-helical tail piece on the C terminus of the partner coiled-coil to form the globular region at both ends of the dimer. The assembly properties of truncation constructs are consistent with a 130 Å overlap. Constructs 15T and 14T form dimers of coiled-coils, while construct 12T is a monomer under assembly conditions. Although construct 12T contains both the positive and negative patches along the coiled-coil, it lacks the

overhanging sequence that we propose is required for tailpiece binding. The small tailpiece consisting of many glycine and serine residues might bind along the partner coiled-coil rather than creating a well-defined structure of its own.

### Comparison of the myosin-II dimer with other coiled-coil structures

The myosin-II 15T dimer is distinct from all previous structures of coiled-coil proteins determined by EM, X-ray crystallography or NMR spectroscopy. The subfragment-2 region of the tail of chicken skeletal muscle myosin forms crystalline tubes in 30 mM MgCl<sub>2</sub>. The 2D filtered images showed 61 nm coiled-coils with a pitch of 14.1 nm staggered by a quarter pitch. These coiled-coils are presumably parallel and lack the globular tailpiece regions of the myosin-II dimer.<sup>31</sup> A coiled-coil protein from the ootheca of a praying mantis forms microcrystals about ten unit cells thick. They diffract electrons to better than 1.5 Å and optical diffraction from spot scan EM images extended to 4.3 Å. A projection map was interpreted to show 400 Å coiled-coils with an anti-parallel overlap of about 300 Å.<sup>32</sup>

High-resolution structures show that many coiled-coils are closely similar to the leucine zipper transcription factor GCN4,<sup>25</sup> but with a range of variations, particularly at their ends. The N terminus (residues 2–55) of the tumor suppressor APC forms a parallel, two-chain coiled-coil very similar to GCN4 in spite of substantial differences in sequence.<sup>33</sup> This similarity, observed also in the structure of cortexillin,<sup>26</sup> supports our use of GCN4 as our molecular replacement model and the basis for the model shown in Figure 5. The last ten residues of this APC construct “splay” apart in the crystal structure and interact with a neighboring molecule to form an anti-parallel, tail-to-tail, four-helix bundle. This is thought to be a crystal-packing artifact, which bears no resemblance to the side-by-side anti-parallel dimer of 15T. The C terminus of skeletal muscle tropomyosin forms two different structures. An X-ray structure of a C-terminal construct fused to GCN4 has nine residues of standard coiled-coil, but the C-terminal 22 residues formed two helices that splayed apart, forming a tail-to-tail dimer with another molecule in the crystal.<sup>34</sup> Again, this is thought to be a crystallization artifact. An NMR structure of a 34 C-terminal tropomyosin construct has the last 20 residues diverged into two parallel linear helices.<sup>35</sup> These parallel helices have unconventional residues in the a and d positions (unbranched hydrophobic residues and a Y rather than  $\beta$ -branched residues in the a position and Q, I and A rather than unbranched hydrophobic residues at the d position). The myosin-II 15T has conventional residues in the a and d positions and is unlikely to make such a parallel strand structure.

## Future prospects

Although a chemically reasonable model could be proposed for the first assembly intermediate of the myosin-II minifilament (Figure 5), this was not sufficient for solving the X-ray structure by molecular replacement. A higher-resolution map derived by analysis of frozen-hydrated 2D crystals should resolve individual  $\alpha$ -helices in the coiled-coil dimer, define the extent of overlap, resolve the 29 residue tailpiece and provide sufficient detail to guide molecular replacement analysis.

## Materials and Methods

### Protein purification

All myosin-II constructs were expressed in *Escherichia coli*. Construct 15T was purified from the soluble pool of lysed cells by boiling and cation-exchange chromatography, while other tail constructs were purified as described.<sup>4</sup>

### The 3D crystallization trials

Crystallization trials for all the constructs were performed using the vapor-diffusion method. Construct 15T crystallized in hanging drops at 15 °C. The well contained 10% (w/v) PEG 400, 0.1 M Tris (pH 8.5). The protein drop consisted of 2  $\mu$ l of a protein solution at a concentration of 15 mg/ml, 2  $\mu$ l of well buffer and 0.5  $\mu$ l of 30% (v/v) formic acid. Crystals appeared after seven days and grew to a size of 400  $\mu$ m  $\times$  400  $\mu$ m  $\times$  50  $\mu$ m after two to three weeks. Crystals became unstable after 30 days. Since all crystals were grown at 15 °C in an enclosed incubator, the crystals were moved to 23 °C or 4 °C for viewing or mounting.

### X-ray data collection

All data were collected at 100 K on crystals flash-frozen in liquid nitrogen after soaking for less than 10 s in cryoprotectant solution (10% PEG 400, 0.1 M Tris (pH 8.5), 20% (v/v) ethylene glycol). Native data extending to 3.5 Å was collected at the Stanford Synchrotron Radiation Laboratory (SSRL) on beam line 7-1 (Table 1). The data were indexed and integrated with DENZO and scaled with SCALEPACK.<sup>36</sup> The CCP4 suite of programs was used to derive structure factor amplitudes.<sup>37</sup> We calculated and viewed Patterson maps using the *xfft* and *xcontur* modules of the *Xtalview* package.<sup>38</sup> We used the program *O* to build a molecular replacement search model of 15T consisting of the sequence of the last 15 heptads of the *Acanthamoeba* myosin-II tail on the backbone of the GCN4 leucine zipper.<sup>39</sup> A skip residue was introduced at serine 1418 by building an extra residue into the sequence. The model was regularized using *O*, and the energy was minimized using XPLOR.<sup>40</sup> In addition to the GCN4 model, we searched with simpler alanine models, C $\alpha$  backbones and single  $\alpha$ -helices as short as 12 residues alone to locate the coiled-coil in the event of curvature in the myosin coiled-coil or changes in-register between the  $\alpha$ -helices. We used these models to search for molecular replacement solutions using the programs AMoRe,<sup>41</sup> EPMR,<sup>42</sup> and CNS.<sup>43</sup> Candidate solutions were displayed using *O*, and the electrostatic

potential was rendered using GRASP.<sup>44</sup> We are grateful to Yu Li in Carolyn Cohen's laboratory, who attempted molecular replacement on our X-ray data using AMoRe and cortaxillin-based coiled-coil models, unfortunately without success.

### X-ray phasing

Potential heavy-atom derivatives were prepared by soaking or co-crystallizing 15T crystals with a variety of heavy-atom compounds. We tested crystals of both native 15T and 15T with single cysteine point mutants at residues S1410, Q1435, S1449 and X1510. The crystals were very sensitive to solvent changes and did not diffract. We also created methionine point mutants at residues L1376, I1383, V1394, S1449 and I1472 and prepared selenomethionine crystals for MAD data collection. Although fluorescence scans indicated that selenium was incorporated in the sample, the resulting data did not allow us to locate the selenium. We presume that either the selenium atoms were bound at very mobile positions or the data were too noisy to identify the small anomalous change due to two selenium atoms per molecule.

### The 2D crystallization trials and electron microscopy

The 2D crystals were grown directly on EM grids using a technique similar to that described by Auer *et al.*<sup>45</sup> Copper EM grids were coated with a thin layer of carbon and were rendered hydrophilic by glow discharge for 20 s. We incubated 1  $\mu$ l of 15T (1 mg/ml) with 2  $\mu$ l of 9% PEG 400, 0.1 M Tris (pH 8.5) on the carbon surface for two minutes. The grids were then blotted to remove most of the sample and stained with 1% (w/v) uranyl acetate containing 1% (w/v) glucose. Grids were examined by transmission EM with a Philips/FEI CM-120 electron microscope at 100 kV using magnifications between 30,000 $\times$  and 52,000 $\times$ .<sup>46</sup> Since less than 5% of the visible crystals were sufficiently ordered, an initial screen of the grid was obtained by recording images of the best-looking crystals at 0° tilt. The coordinates of each crystal were saved using the computer-controlled stage while the micrographs were developed and checked for optical diffraction. Using the saved coordinates, we returned to the location of the crystals with the best optical diffraction and recorded up to six low-dose images of the same crystal at various tilt angles, starting near 55°.

### Image processing

Images with a visible (2, 2) reflection by optical diffraction were selected for image processing. The region

**Table 2.** EM data analysis summary

Parameter	Value
No. images	58
Unique crystals	10
Unit cell (Å)	89.1, 65.5
Plane group	<i>c</i> 12
Tilt range (deg.)	0–55
Underfocus range (Å)	–8000 to –12,350
No. reflections	1708
No. unique reflections	598
Average phase error (deg.)	14.6
Resolution	
In-plane (Å)	13.7
In <i>z</i> (Å)	35

of the micrograph containing the crystal was digitized using a microdensitometer with a step size of 10  $\mu\text{m}$  and processed using the MRC suite of programs<sup>47</sup> as described.<sup>46</sup> After two rounds of image filtering and lattice unbending, we obtained a continuous region of approximately 0.5  $\mu\text{m}^2$  of useful data per crystal. Multiple images were shifted to the phase origin for plane group *c2* and merged to increase the signal-to-noise ratio and to filter out single-image artifacts. The average amplitudes and phases were used to calculate a projection map using the CCP4 suite of programs.<sup>37</sup> To reconstruct the 3D structure, 58 images were recorded at tilt angles between 0° and 55° (Table 2). After obtaining the best set of merged data consisting of *h*, *k*, *z\**, phase and amplitude, continuous lattice lines were derived by interpolation along *z\**. To calculate an electron density map, the continuous lattice lines were sampled at discrete points assuming a crystal thickness of 115 Å based on the *c* dimension of the 3D crystal. The 3D density map was then calculated by Fourier transformation, contoured at the appropriate molecular volume and visualized using O<sup>39</sup> and AVS software.<sup>48</sup>

## Acknowledgements

We thank Anchi Cheng and Kelly Dryden for assistance with electron microscopy, Bob Robinson and Senyon Choe for assistance with X-ray crystallography and Michael E. Pique for assistance with preparation of Figure 4. This work has been supported by NIH grants HL48908 (to M.Y.) and GM26338 (to T.D.P.). During this work, M.Y. was the recipient of a Clinical Scientist Award in Translational Research from the Burroughs Wellcome Fund.

## References

- Sinard, J. H., Stafford, W. F. & Pollard, T. D. (1989). The mechanism of assembly of *Acanthamoeba* myosin-II minifilaments: minifilaments assemble by three successive dimerization steps. *J. Cell Biol.* **109**, 1537–1547.
- Sinard, J. H., Rimm, D. L. & Pollard, T. D. (1990). Identification of functional regions on the tail of *Acanthamoeba* myosin-II using recombinant fusion proteins. II. Assembly properties of tails with NH<sub>2</sub>- and COOH-terminal deletions. *J. Cell Biol.* **111**, 2417–2426.
- Rimm, D. L., Kaiser, D. A., Bhandari, D., Maupin, P., Kiehart, D. P. & Pollard, T. D. (1990). Identification of functional regions on the tail of *Acanthamoeba* myosin-II using recombinant fusion proteins. I. High resolution epitope mapping and characterization of monoclonal antibody binding sites. *J. Cell Biol.* **111**, 2405–2416.
- Turbedsky, K. & Pollard, T. D. (2005). Definition of the C-terminal residues of *Acanthamoeba* myosin-II required to form coiled-coils, dimers and octameric mini-filaments. *J. Mol. Biol.* (this issue).
- Hammer, J. A., III, Bowers, B., Paterson, B. M. & Korn, E. D. (1987). Complete nucleotide sequence and deduced polypeptide sequence of a nonmuscle myosin heavy chain gene from *Acanthamoeba*: evidence of a hinge in the rodlike tail. *J. Cell Biol.* **105**, 913–925.
- McLachlan, A. D. & Karn, J. (1982). Periodic charge distributions in the myosin rod amino acid sequence match cross-bridge spacings in muscle. *Nature*, **299**, 226–231.
- McLachlan, A. D. & Karn, J. (1983). Periodic features in the amino acid sequence of nematode myosin rod. *J. Mol. Biol.* **164**, 605–626.
- Conway, J. F. & Parry, D. A. (1990). Structural features in the heptad substructure and longer range repeats of two-stranded alpha-fibrous proteins. *Int. J. Biol. Macromol.* **12**, 328–334.
- Reisler, E. (1980). Kinetic studies with synthetic myosin minifilaments show the equivalence of acto-myosin and acto-HMM ATPases. *J. Biol. Chem.* **255**, 9541–9544.
- Reisler, E., Cheung, P., Oriol-Audit, C. & Lake, J. A. (1982). Growth of synthetic myosin filaments from myosin minifilaments. *Biochemistry*, **21**, 701–707.
- Cohen, C. & Parry, D. A. D. (1998). A conserved C-terminal assembly region in paramyosin and myosin rods. *J. Struct. Biol.* **122**, 180–187.
- Sohn, R. L., Vikstrom, K. L., Strauss, M., Cohen, C., Szent-Gyorgyi, A. G. & Leinwand, L. A. (1997). A 29 residue region of the sarcomeric myosin rod is necessary for filament formation. *J. Mol. Biol.* **266**, 317–330.
- Ikebe, M., Komatsu, S., Woodhead, J. L., Mabuchi, K., Ikebe, R., Saito, J. *et al.* (2001). The tip of the coiled-coil rod determines the filament formation of smooth muscle and nonmuscle myosin. *J. Biol. Chem.* **276**, 30293–30300.
- Rovner, A. S., Fagnant, P. M., Lowey, S. & Trybus, K. M. (2002). The carboxyl-terminal isoforms of smooth muscle myosin heavy chain determine thick filament assembly properties. *J. Cell Biol.* **156**, 113–123.
- Kuznicki, J., Côté, G. P., Bowers, B. & Korn, E. D. (1985). Filament formation and actin-activated ATPase activity are abolished by proteolytic removal of a small peptide from the tip of the tail of the heavy chain on *Acanthamoeba* myosin II. *J. Biol. Chem.* **260**, 1967–1972.
- Huxley, H. E. (1963). Electron microscopic studies of the structure of natural and synthetic protein filaments from striated muscles. *J. Mol. Biol.* **7**, 281–308.
- Huxley, H. E. & Brown, W. (1967). The low-angle X-ray diagram of vertebrate striated muscle and its behavior during contraction and rigor. *J. Mol. Biol.* **30**, 383–434.
- Stewart, M. & Kensler, R. W. (1986). Arrangement of myosin heads in relaxed thick filaments from frog skeletal muscle. *J. Mol. Biol.* **192**, 831–851.
- Squire, J., Cantino, M., Chew, M., Denny, R., Harford, J., Hudson, L. & Luther, P. (1998). Myosin rod-packing schemes in vertebrate muscle thick filaments. *J. Struct. Biol.* **122**, 128–138.
- Whitby, F. G., Kent, H., Stewart, F., Stewart, M., Xie, X., Hatch, V. *et al.* (1992). Structure of tropomyosin at 9 ångströms resolution. *J. Mol. Biol.* **227**, 441–452.
- Crick, F. H. C. (1953). The packing of alpha-helices: simple coiled-coils. *Acta Crystallog.* **6**, 689–697.
- Cohen, C. & Holmes, K. C. (1963). X-ray diffraction evidence for  $\alpha$ -helical coiled-coils in native muscles. *J. Mol. Biol.* **6**, 423–432.

23. Phillips, G. N., Jr (1992). What is the pitch of the  $\alpha$ -helical coiled coil? *Proteins: Struct. Funct. Genet.* **14**, 425–429.
24. Seo, J. & Cohen, C. (1993). Pitch diversity in  $\alpha$ -helical coiled coils. *Proteins: Struct. Funct. Genet.* **15**, 223–234.
25. O'Shea, E. K., Klemm, J. D., Kim, P. S. & Alber, T. (1991). X-ray structure of the GCN4 leucine zipper, a two-stranded, parallel coiled coil. *Science*, **254**, 539–544.
26. Burkhard, P., Kammerer, R. A., Steinmetz, M. O., Bourenkov, G. P. & Aebi, U. (2000). The coiled-coil trigger site of the rod domain of cortexillin I unveils a distinct network of interhelical and intrahelical salt bridges. *Struct. Fold. Des.* **8**, 223–230.
27. Hayat, M. A. & Miller, S. E. (1990). *Negative Staining*, McGraw-Hill, New York.
28. Burkhard, P., Steinmetz, M. O., Schulthess, T., Landwehr, R., Aebi, U. & Kammerer, R. A. (1998). Crystallization and preliminary X-ray diffraction analysis of the 190-A-long coiled-coil dimerization domain of the actin-bundling protein cortexillin I from *Dictyostelium discoideum*. *J. Struct. Biol.* **122**, 293–296.
29. Pollard, T. D. (1982). Structure and polymerization of *Acanthamoeba* myosin-II filaments. *J. Cell Biol.* **95**, 816–825.
30. Whitby, F. G. & Phillips, G. N., Jr (2000). Crystal structure of tropomyosin at 7 ångströms resolution. *Proteins: Struct. Funct. Genet.* **38**, 49–59.
31. Quinlan, R. A. & Stewart, M. (1987). Crystalline tubes of myosin subfragment-2 showing the coiled-coil and molecular interaction geometry. *J. Cell Biol.* **105**, 403–415.
32. Bullough, P. A. & Tulloch, P. A. (1990). High resolution spot-scan electron microscopy of microcrystals of an  $\alpha$ -helical coiled-coil protein. *J. Mol. Biol.* **105**, 161–173.
33. Day, C. L. & Alber, T. (2000). Crystal structure of the amino-terminal coiled-coil domain of the APC tumor suppressor. *J. Mol. Biol.* **301**, 147–156.
34. Li, Y., Mui, S., Brown, J. H., Strand, J., Reshetnikova, L., Tobacman, L. S. & Cohen, C. (2002). The crystal structure of the C-terminal fragment of striated-muscle alpha-tropomyosin reveals a key troponin T recognition site. *Proc. Natl Acad. Sci. USA*, **99**, 7378–7383.
35. Greenfield, N. J., Swapna, G. V. T., Huang, Y., Palm, T., Graboski, S., Montelione, G. T. & Hitchcock-DeGregori, S. E. (2003). The structure of the carboxyl terminus of striated  $\alpha$ -tropomyosin in solution reveals an unusual parallel arrangement of interacting  $\alpha$ -helices. *Biochemistry*, **42**, 614–619.
36. Otwinowski, Z. & Minor, W. (1998). Processing of X-ray diffraction data collected in oscillation mode. *Methods Enzymol.* **276**, 307–326.
37. Collaborative Computational Project, Number 4. (1994). The CCP4 suite: programs for protein crystallography. *Acta Crystallog. sect. D*, **50**, 760–763.
38. McRee, D. E. (1999). XtalView/Xfit—a versatile program for manipulating atomic coordinates and electron density. *J. Struct. Biol.* **125**, 156–165.
39. Jones, T. A., Zou, J. Y., Cowan, S. W. & Kjeldgaard, M. (1993). Improved methods for building protein models in electron density maps and the location of errors in these models. *Acta Crystallog. sect. D*, **49**, 147–157.
40. Brünger, A. T. (1993). *XPLOR Version 3.1*, Yale University Press, New Haven, CT.
41. Navaza, J. (1994). AMoRe: an automated package for molecular replacement. *Acta Crystallog. sect. A*, **50**, 157–163.
42. Kissinger, C. R., Gehlhaar, D. K. & Fogel, D. B. (1999). Rapid automated molecular replacement by evolutionary search. *Acta Crystallog. sect. D*, **55**, 484–491.
43. Brünger, A. T., Adams, P. D., Clore, G. M., DeLano, W. L., Gros, P., Grosse-Kunstleve, R. W. *et al.* (1998). Crystallography & NMR system: a new software suite for macromolecular structure determination. *Acta Crystallog. sect. D*, **54**, 905–921.
44. Nicholls, A., Sharp, K. A. & Honig, B. (1991). Protein folding and association: insights from the interfacial and thermodynamic properties of hydrocarbons. *Proteins: Struct. Funct. Genet.* **11**, 281–296.
45. Auer, M., Scarborough, G. A. & Kühlbrandt, W. (1999). Surface crystallisation of the plasma membrane H<sup>+</sup>-ATPase on a carbon support film for electron crystallography. *J. Mol. Biol.* **287**, 961–968.
46. Yeager, M., Unger, V. M. & Mitra, A. K. (1999). Three-dimensional structure of membrane proteins determined by two-dimensional crystallization, electron cryomicroscopy, and image analysis. *Methods Enzymol.* **294**, 135–180.
47. Crowther, R. A., Henderson, R. & Smith, J. M. (1996). MRC image processing programs. *J. Struct. Biol.* **116**, 9–16.
48. Sheehan, B., Fuller, S. D., Pique, M. E. & Yeager, M. (1996). AVS software for visualization in molecular microscopy. *J. Struct. Biol.* **116**, 99–106.

Edited by W. Baumeister

(Received 25 August 2004; accepted 18 October 2004)